EXTENDED PDF FORMAT
SPONSORED BY
usb
www.usbweb.com

Coherent Control of Decoherence
Matthijs P. A. Branderhorst, *et al.*
Science **320**, 638 (2008);
DOI: 10.1126/science.1154576

The following resources related to this article are available online at www.sciencemag.org (this information is current as of May 8, 2008):

Updated information and services, including high-resolution figures, can be found in the online version of this article at:
http://www.sciencemag.org/cgi/content/full/320/5876/638

Supporting Online Material can be found at:
http://www.sciencemag.org/cgi/content/full/320/5876/638/DC1

This article **cites 34 articles**, 3 of which can be accessed for free:
http://www.sciencemag.org/cgi/content/full/320/5876/638#otherarticles

This article appears in the following **subject collections**:
Physics
http://www.sciencemag.org/cgi/collection/physics

Information about obtaining **reprints** of this article or about obtaining **permission to reproduce this article** in whole or in part can be found at:
http://www.sciencemag.org/about/permissions.dtl

Downloaded from www.sciencemag.org on May 8, 2008

Science (print ISSN 0036-8075; online ISSN 1095-9203) is published weekly, except the last week in December, by the American Association for the Advancement of Science, 1200 New York Avenue NW, Washington, DC 20005. Copyright 2008 by the American Association for the Advancement of Science; all rights reserved. The title *Science* is a registered trademark of AAAS.

waste-heat recovery applications. These materials are synthesized via ball milling, followed by dc hot pressing. The ZT enhancement comes mainly from a large reduction in the phonon thermal conductivity but also benefits from a reduction of bipolar contributions to the electronic thermal conduction at high temperatures. In the past, ZT enhancements have been reported in superlattice structures because of phonon thermal conductivity reduction. Our study suggests that a similar mechanism can be reproduced in random nanostructured bulk materials. Unlike superlattices and bulk crystals, a nanostructured BiSbTe alloy displays nearly isotropic ZT values. We further confirmed ZT enhancements by measuring the temperature difference created by unicouple devices constructed out of the materials for hot-side temperature maintained between 50° to 150°C. The nanostructure synthesis method that we developed is a low-cost technique and can be readily scaled for mass production. These results provide a cost-effective means to improve the performance of thermoelectric materials.

References and Notes

1. D. M. Rowe, Ed. *CRC Handbook of Thermoelectrics* (CRC, Boca Raton, FL, 1995).
2. H. J. Goldsmid, *Thermoelectric Refrigeration* (Plenum, New York, 1964).
3. T. M. Tritt, Ed. *Semiconductors and Semimetals, Recent Trends in Thermoelectric Materials Research: Part One to Three* (Academic, San Diego, CA, 2001), vol. 69 to 71.
4. R. Venkatasubramanian, E. Siivola, T. Colpitts, B. O'Quinn, *Nature* **413**, 597 (2001).
5. T. C. Harman, P. J. Taylor, M. P. Walsh, B. E. LaForge, *Science* **297**, 2229 (2002).
6. K. F. Hsu *et al.*, *Science* **303**, 818 (2004).
7. J. P. Fluerial, T. Caillat, A. Borshchevsky, in *Proceedings of the 13th International Conference on Thermoelectrics*, Kansas City, MO, 30 August to 1 September 1994 (AIP, New York, 1995), pp. 40–44.
8. G. Chen, *Phys. Rev. B* **57**, 14958 (1998).
9. M. S. Dresselhaus *et al.*, *Adv. Mater.* **19**, 1043 (2007).
10. X. B. Zhao *et al.*, *Appl. Phys. Lett.* **86**, 062111 (2005).
11. X. F. Tang, W. J. Xie, H. Li, W. Y. Zhao, Q. J. Zhang, *Appl. Phys. Lett.* **90**, 012102 (2007).
12. Bulk p-type BiSbTe alloy ingots were loaded into a jar with balls inside the argon-filled glove box to avoid oxidation of the nanopowder. The jar was loaded into a ball mill and processed for several hours. When the nanopowder was ready, it was loaded into 1.25- to 2.5-cm (inner diameter) dies and compacted into a 100% dense solid NC bulk sample by a hot press. Samples are available for testing upon request.
13. We cut hot-pressed NC bulk pellets into blocks (2 mm by 3 mm by 1 mm) that were ground down into smaller blocks (2 mm by 3 mm by 0.002 mm) using a mechanical tripod polisher. We then glued the sample to a copper grid and milled it using a precision ion polishing system (Gatan Inc., Warrendale, Pennsylvania, USA) for 30 min, with incident energy of 3.2 kV and beam current of 15 μA at an incident angle of 3.5°.
14. T. C. Harman, S. E. Miller, H. L. Goeing, *Bull. Am. Phys. Soc.* **30**, 35 (1955).
15. T. Thonhauser, G. S. Jeon, G. D. Mahan, J. O. Sofo, *Phys. Rev. B* **68**, 205207 (2003).

16. The work is supported by the U.S. Department of Energy (DOE) grant no. DE-FG02-00ER45805 (Z.F.R.), DOE grant no. DE-FG02-02ER45977 (G.C.), NSF–Nanoscale Interdisciplinary Research Team grant no. 0506830 (G.C., Z.F.R., and M.S.D.), National Science Foundation of China project no. 50528203 (J.M.L. and Z.F.R.), and the Ministry of Science and Technology of China project no. 2006CB921802 (J.M.L.). G.C. and Z.F.R. are cofounders of GMZ Energy, Inc.

13 February 2008; accepted 11 March 2008
Published online 20 March 2008;
10.1126/science.1156446
Include this information when citing this paper.

REPORTS

Coherent Control of Decoherence

Matthijs P. A. Branderhorst,[1] Pablo Londero,[1] Piotr Wasylczyk,[1] Constantin Brif,[2] Robert L. Kosut,[3] Herschel Rabitz,[2] Ian A. Walmsley[1]

Manipulation of quantum interference requires that the system under control remains coherent, avoiding (or at least postponing) the phase randomization that can ensue from coupling to an uncontrolled environment. We show that closed-loop coherent control can be used to mitigate the rate of quantum dephasing in a gas-phase ensemble of potassium dimers (K_2), which acts as a model system for testing the general concepts of controlling decoherence. Specifically, we adaptively shaped the light pulse used to prepare a vibrational wave packet in electronically excited K_2, with the amplitude of quantum beats in the fluorescence signal used as an easily measured surrogate for the purpose of optimizing coherence. The optimal pulse increased the beat amplitude from below the noise level to well above it, and thereby increased the coherence life time as compared with the beats produced by a transform-limited pulse. Closed-loop methods can thus effectively identify states that are robust against dephasing without any previous information about the system-environment interaction.

Interference is one of the hallmarks of quantum physics, and its presence is generally taken to demarcate the boundary between quantum and classical behavior. Controlling a quantum system consists of manipulating the relative amplitudes and phases of different distinct quantum states of the system, in order to achieve some objective, such as a particular functional operation or an increased yield of a particular outcome. The map from the optimal set of controls to the interference pattern of quantum probability amplitudes, which generates the desired outcome, is typically very complex. Therefore, iterative adaptive control (*1*), in which the system is incorporated into a feedback loop, is one of the most powerful tools for optimizing quantum control results in the laboratory. This method has wide currency and is applicable to a variety of very different physical and chemical systems and processes. For example, the closed-loop approach enabled the experimenters to coherently control the shape of an atomic electron's wave function (*2*), energy flow in a photosynthetic complex (*3*), polarization-sensitive photoionization channels (*4*), isotope-selective photoionization of molecules (*5*), photoisomerization of the retinal molecule in bacteriorhodopsin (*6*), high-harmonic generation of coherent soft x-rays (*7*), selective photodissociation and rearrangement of molecular bonds (*8*), and large-amplitude oscillations in C_{60} (*9*).

The effectiveness of coherent control is compromised by the coupling of the system to an uncontrolled environment, which disturbs in a random fashion the delicate quantum phases that define the state of the system. The time scales for decoherence vary widely. For example, the dephasing times for electronic dipole excitations range from the femtosecond to nanosecond regime, as a result of coupling to local phonon modes and spontaneous emission; those for spin (magnetic-dipole) excitations vary from microseconds to milliseconds, resulting from coupling to other spins in the sample or from collisions.

Typically, the quantum system is prepared in an initial state by the controller. The system then undergoes some free evolution, during which it is affected by the environment: Both loss of quantum coherence and dissipation of energy may occur. The inability to sustain the phase and amplitude relationships between the eigenstates of the system renders the controls ineffective. Any realistic goal for quantum control therefore requires sustaining the coherence in the system, and it is an open question whether and how this is possible in the face of dephasing perturbations. In particular, is there an optimal strategy to counter the effects of the environment? Protecting the quantum coherence is an important goal in various systems and processes. For example, it was recently discovered (*10*) that the coherence of excited electronic states plays an important role in biochemical processes, such as energy harvesting in photosynthesis. Similarly, the coherence of multiparticle superposition states is crucial for the implementation of quantum information processing (*11*, *12*). It is in this context that the control of decoherence has been studied most com-

[1]Clarendon Laboratory, University of Oxford, Parks Road, Oxford OX1 3PU, UK. [2]Department of Chemistry, Princeton University, Princeton, NJ 08544, USA. [3]SCSolutions, 1261 Oakmead Parkway, Sunnyvale, CA 94085, USA.

*To whom correspondence should be addressed. E-mail: walmsley@physics.ox.ac.uk

Downloaded from www.sciencemag.org on May 8, 2008

prehensively, leading to the concepts of quantum error correction (QEC) (*13*, *14*), dynamical decoupling (DD) (*15*, *16*), and decoherence-free subspaces (DFSs) (*17*). These approaches either actively correct deviations of the system evolution from the one expected (QEC) or decouple the system from the environment, either actively (DD) or passively (DFS).

We wondered whether the tools of coherent control could themselves be used to inhibit dephasing. Because decoherence is ubiquitous, this is a far-reaching question, and the (perhaps) unexpected answer is that they can. We demonstrate experimentally some general principles that have broad application across many fields where maintaining quantum coherence is important. We chose a simple initial problem: maintaining the coherence of a prepared quantum state, without directing that coherence toward achievement of any particular function. This approach allowed us to explore experimentally some of the fundamental issues and to learn from the controls the mechanism by which they succeeded. The results give confidence that the approach will be widely applicable. For example, recent theoretical studies suggest that optimal coherent control can help increase the purity of quantum states in dissipative atomic and molecular systems (*18*, *19*), suppress dephasing due to electron-phonon scattering in semiconductor quantum dots (*20*, *21*), reduce the rate of dissipation in a spin-boson model in the strong coupling regime (*22*), suppress various channels of electronic and vibrational dissipation and dephasing in molecules (*23*), and protect coherence in spin-based quantum gates (*21*, *24*). An important conclusion of these theoretical studies, which is confirmed by our experimental results, is that the coherent preparation of quantum states can substantially alter the outcome of the subsequent nonunitary dynamics induced by the uncontrolled environment. Moreover, the method of closed-loop optimization successfully implemented in the present experiment has been proven to be a very efficient tool for finding optimal coherent controls in the laboratory. The generality of the closed-loop approach should make it useful for management of coherence in a variety of problems (e.g., in those mentioned above), provided that easily measurable markers for coherence are available. These future applications depend on the progress in developing laboratory techniques for coherent manipulation and measurement of the corresponding quantum systems.

First, we wish to consider a system that can be analyzed completely and is experimentally tractable, yet is of sufficient complexity that its decoherence dynamics are essentially generic, so that the methods we use and results we obtain for this system are in principle applicable to a wide range of more complex situations. The criteria for identifying such a system are that there exists a set of feasible laboratory measurements that maps a particular degree of freedom of the system to experimental outcomes and that the unobserved part of the system has the known properties of a dephasing environment. We take the space of the corresponding set of observables to define the system itself. This essentially pragmatic approach is required because the system and environment are necessarily coupled; hence, there is no clear separation of the overall Hilbert space. A key criterion for the unobserved part of the entity (that is, the environment) is that it is of sufficient size that the entropy flow is essentially one way, with no environmentally induced revivals of the system coherence on the time scale of the experiment (*25*). Moreover, the spectrum of the environment must be broad and unstructured, thereby providing a short correlation time.

Second, a critical factor in the operation of a control loop is identifying an experimentally accessible, faithful measure of the objective characteristic, around which a control loop can be implemented. Standard measures of coherence—such as the purity of the state of the system, $P = \mathrm{Tr}(\rho^2)$, or the von Neumann entropy, $S = -\mathrm{Tr}(\rho \ln \rho)$—are nonlinear functions of the state operator ρ and can therefore be estimated only via joint measurements on pairs of identically prepared systems (*23*, *26*) or calculated from state estimates determined by means of quantum state tomography (*27*). These approaches are technically challenging or may require too much data to be of use in a reasonable bandwidth feedback loop. Therefore, simple measures must be found that may act as a marker for coherence or a coherence surrogate (CS). That is, for a range of values of the CS around a certain threshold, coherence of the system is guaranteed and otherwise ruled out. One CS is the degree to which the system is localized or confined to a small region of configuration or phase space, because this property necessarily implies that the quantum state is a coherent superposition of the energy eigenstates of the system (*28*). A possible strategy to control decoherence is therefore to measure the localization of a wave packet at some time after its excitation and then to use this information in a feedback loop that changes the shape of the packet in such a manner as to maximize the longevity of its coherence. This

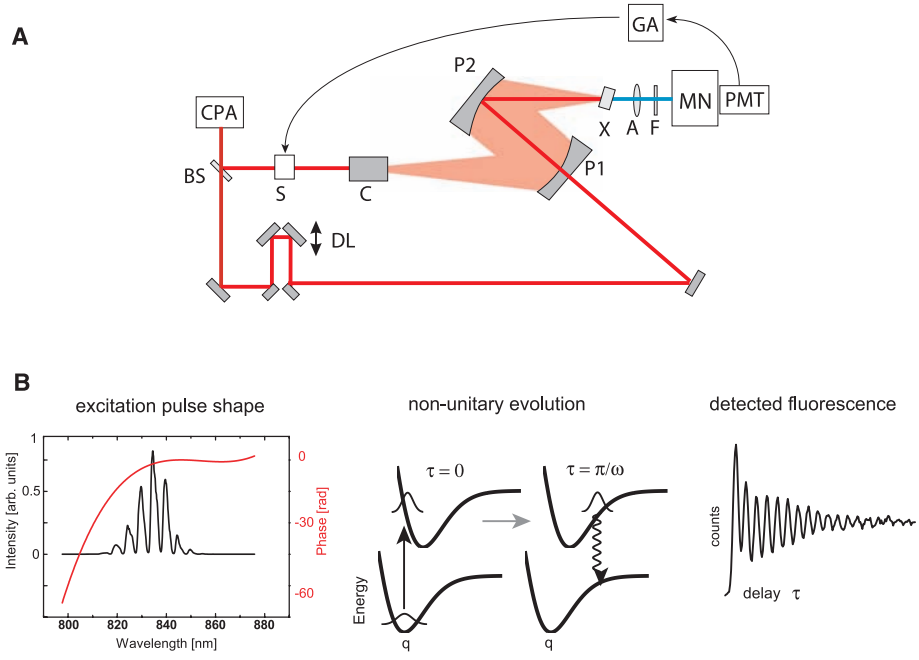

Fig. 1. (**A**) Apparatus for control and measurement of the vibrational wave packet states of potassium dimers and (**B**) excitation of a shaped vibrational wave packet and its detection at the outer turning point. A pulse from a chirped-pulse-amplified mode-locked Ti:sapphire laser system (CPA) is shaped via a Fourier-plane pulse shaper (S) and incident on a cell (C) containing a gas of K_2 molecules at 400°C. Absorption generates a wave packet in the lowest excited electronic state $A^1\Sigma_u^+$ of the molecules. Fluorescence from this state is collected in the near-forward direction by two off-axis parabolic mirrors (P1 and P2) and focused on a nonlinear crystal (X) where it is mixed with a portion of the unshaped laser pulse [the gate pulse, derived from the laser pulse by a beamsplitter (BS)] that has been sent through an adjustable delay line (DL). The resulting frequency-upconverted radiation is imaged (depicted as "A") through a broadband filter (F) onto the slits of a monochromator (MN) after which it is detected by a photomultiplier tube (PMT). Quantum beats are observed in the time- and frequency-resolved fluorescence as the vibrational wave packet oscillates in the excited electronic state potential, as illustrated in the middle panel of (B). The resulting detected signal is shown in the right panel of (B). The time- and frequency-resolved signal shows quantum beats as a function of the time delay τ between the gate pulse and excitation pulse, which have a periodicity $2\pi/\omega$ corresponding to the wave packet oscillation frequency ω. The signal is processed in a computer with a genetic algorithm (GA) and used to reshape the pulse that excites the wave packet in the dimers. This closed-loop control system searches for a wave packet shape that is most immune to the dephasing caused by the rotational-vibrational coupling. The optimal pulse profile (red line) is shown in (B) on the left.

Downloaded from www.sciencemag.org on May 8, 2008

approach is comparable to searching for a DFS for the system, without knowing a priori that such a subspace exists, even in principle. This capability is important for the common situation in which the system-environment coupling is not known in sufficient detail to formally address the question.

Among the simplest physical systems that satisfy these requirements is a diatomic molecule (*29*, *30*). Here, the system is the vibrational mode of internuclear motion in the excited electronic state. The wave packet localization is detected by means of time- and frequency-resolved fluorescence that exhibits (for localized states) quantum beats, the visibility of which forms the control signal. The visibility is calculated from the experimental data as the normalized difference of the fluorescence intensity at the peak and at the valley of a specific quantum beat. This CS requires only two data points as input to the control loop, and the value of the visibility ranges between zero (no quantum beats) and unity or 100% (full modulation of the fluorescence intensity). Measurement of the fluorescence projects out only the vibrational motion in the excited electronic state of the molecule. The reservoir is the rotational degree of freedom of the molecule, which is coupled to the vibrational motion through the moment of inertia. Changes in the moment of inertia as the molecule vibrates cause dephasing of the vibrational state. The distribution of population in the reservoir degree of freedom, which at high temperatures forms a quasi-continuum, is unaffected by this coupling to the system. Note that the quantum state of a system, and all state characteristics such as the coherence, indeed describe an ensemble of identical systems. Correspondingly, in the present case, although dephasing of the vibrational wave packet is caused by a purely intramolecular process of the vibration-rotation interaction, the coherence of the vibrational quantum system refers to the ensemble of molecules. This reference to the ensemble is true as well for all quantitative measures of the coherence, which are functions of the quantum state operator, and for the CS, which is deduced from the ensemble average of an observable.

The apparatus used to control the initial shape of the wave packet, and thus to manage the rate at which it dephases, is shown in Fig. 1A. Optical pulses of ~90-fs duration, whose mean wavelength is tuned to the lowest electronic transition of the potassium dimer, are shaped by means of an acousto-optic modulator in a Fourier-plane shaper before exciting a vibrational wave packet in the $^1\Sigma_u^+$ electronic state of the molecules, which were kept in the gas phase at ~400°C. The vibrational wave packet produced by the optical pulse in the excited electronic state has a higher purity than the initial thermal vibrational state in the ground electronic state because of the selectivity of the Franck-Condon transition. The electronically excited molecules vibrate with a period of ~500 fs, and the fluorescence emanating from transitions near the outer turning point of the wave packet's motion exhibits quantum beats with this period (Fig. 1B). The beats decay in amplitude (Fig. 2), as a result of several physical effects. The dominant effect is dephasing resulting from the rotational bath, which has an estimated decay time of 3 ps for this molecule and temperature (*30*). Delocalization of the wave packet due to the anharmonic character of the vibrational potential also causes a reduction in the beat visibility. This purely Hamiltonian evolution cannot be distinguished from dephasing by the CS, though the purity of the state remains constant for this kind of dynamics. Hence, the CS provides a sufficient but not necessary condition for the existence of coherence: The absence of localization does not necessarily imply that the state of the vibrational mode is completely mixed (corresponding to a vibrational density matrix with zero off-diagonal elements), whereas the presence of localization certainly indicates that the state is not completely mixed. The time scale for anharmonic delocalization is ~12 ps, based on the known molecular potentials (*31*), which is much longer than the dephasing time due to rotational-vibrational coupling. Collisional dephasing of the vibrations is negligible in a low-density gas at this temperature and pressure. Finally, the spin-orbit coupling of the $^1\Sigma_u^+$ and $^3\Pi_u$ states causes a loss of population to an electronic state that is not detected by our fluorescence measurements (*32*). The time scale for this process to occur in the present system is many tens of picoseconds.

The control protocol consists of a measurement of the visibility of the quantum beats near a delay of 7.5 ps after exciting the wave packet. This delay occurs at period 15 of the wave packet oscillations and corresponds to about 3.8 times

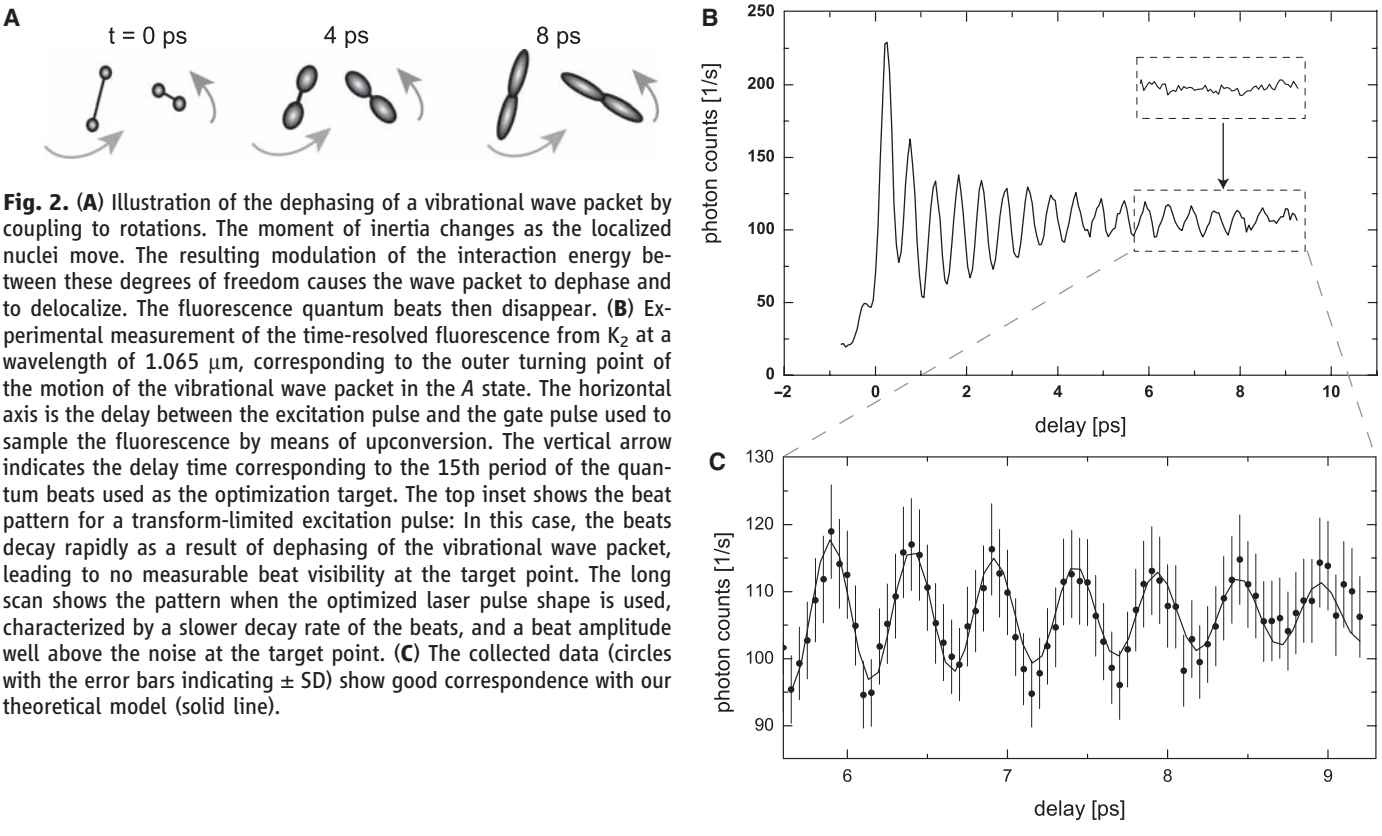

Fig. 2. (**A**) Illustration of the dephasing of a vibrational wave packet by coupling to rotations. The moment of inertia changes as the localized nuclei move. The resulting modulation of the interaction energy between these degrees of freedom causes the wave packet to dephase and to delocalize. The fluorescence quantum beats then disappear. (**B**) Experimental measurement of the time-resolved fluorescence from K_2 at a wavelength of 1.065 μm, corresponding to the outer turning point of the motion of the vibrational wave packet in the *A* state. The horizontal axis is the delay between the excitation pulse and the gate pulse used to sample the fluorescence by means of upconversion. The vertical arrow indicates the delay time corresponding to the 15th period of the quantum beats used as the optimization target. The top inset shows the beat pattern for a transform-limited excitation pulse: In this case, the beats decay rapidly as a result of dephasing of the vibrational wave packet, leading to no measurable beat visibility at the target point. The long scan shows the pattern when the optimized laser pulse shape is used, characterized by a slower decay rate of the beats, and a beat amplitude well above the noise at the target point. (**C**) The collected data (circles with the error bars indicating ± SD) show good correspondence with our theoretical model (solid line).

Downloaded from www.sciencemag.org on May 8, 2008

the measured dephasing time τ_d for the vibrational state excited by the transform-limited pulse. Before the start of the search (i.e., for the transform-limited excitation pulse), no quantum beats were visible in the signal at this delay (Fig. 2B, inset). We used an evolutionary algorithm to search through a variety of wave packet shapes (by changing the shape of the excitation pulse) and found an improvement of the quantum-beat visibility from zero to ~7%, or more than four times the noise level. Repeating this experiment for several different time delays (1.9, 3.8, and 5.6 ps) after the excitation pulse produced similar results (with different optimal pulse shapes), showing that the control pulse shape was able to affect the longevity of the localization of the vibrational wave packet. In order to quantify this effect, and to determine whether controlling the beat visibility was correlated with controlling the decay time of the wave packet's coherence, we measured the decay rate by fitting a damped sinusoid to a full fluorescence beat pattern for each control pulse shape (Fig. 3A). The decay time measured for the optimal control pulse found by the genetic algorithm was about 3.2 ps (i.e., about 1.6 times τ_d). This shows that the details of the wave packet shape affect the subsequent dephasing dynamics. Given that the environment is at 400°C, it is perhaps unexpected to find that any major changes in the coherence decay time can be attributed to subtle changes in the initial state of the vibrational mode.

To understand the outcome of the closed-loop search, we characterized the electric field of the optimal control pulse (*33*) (Fig. 1B, left). We then performed a series of experiments in which the prominent features of the control pulse fields were examined in turn. For each pulse shape, the decay of the quantum beats was measured and a decay time extracted by fitting the beat pattern to an exponentially damped sinusoid (Fig. 3A). The decay times of the quantum beats for several different pulse shapes are shown in Fig. 3B. First, we examined 10 control pulse shapes with no amplitude modulation but with different values of negative quadratic chirp. The longevity of the quantum beats increased with increasing chirp, the longest decay time [about 4.0 ps (i.e., twice τ_d)] corresponding to the largest negative chirp (-3.1×10^3 fs^2) (Fig. 3B). In contrast, for pulses with positive chirp, the beat decay time decreased as compared with that of the transform-limited pulse (we examined 10 pulse shapes with different values of positive quadratic chirp). The largest negative chirp leads to a decay time longer than that found via the closed-loop control optimization, although the visibility of the quantum beats around 7.5 ps is smaller. The difference between these outcomes arises because the signal guiding the control loop is the amplitude of the quantum beats at a specified time delay, rather than the decay time extracted from the entire beat pattern. Again, this result is a consequence of our strategy to run the control loop with the minimal amount of data necessary. Measuring the entire decay pattern of quantum beats and fitting the obtained result to a damped sinusoid are good methods for analysis, but this requires a very large number of measurements, across 200 different time delays that take about 30 min to complete per control pulse shape. Therefore, it would be impractical to use such a long sequence of measurements as part of the control loop. On the other hand, the beat visibility at just one time delay yields less information about the system behavior than the entire decay curve, but the visibility measurement can be completed in just 20 s and is therefore well suited for use in a high-bandwidth control loop. We observed that although the strategy to run the control loop using the minimal data necessary did not maximize the decay time, it was still very effective in increasing the longevity of coherence. Next, a control pulse shape consisting of a sequence of subpulses—each shorter than the vibrational period, and each without chirp—was applied to the molecules. A small increase in the decay time was observed when the temporal separation between the subpulses was equal to the vibrational period. We concluded from this analysis that negative chirp was the most important characteristic of the closed-loop search outcome.

The mechanism by which the optimally shaped pulse mitigated the dephasing of the vibrational wave packet was identified by analyzing a model of the system based on a rotational-vibrational coupling Hamiltonian for the excited electronic state of the molecule. Within the Born-Oppenheimer approximation,

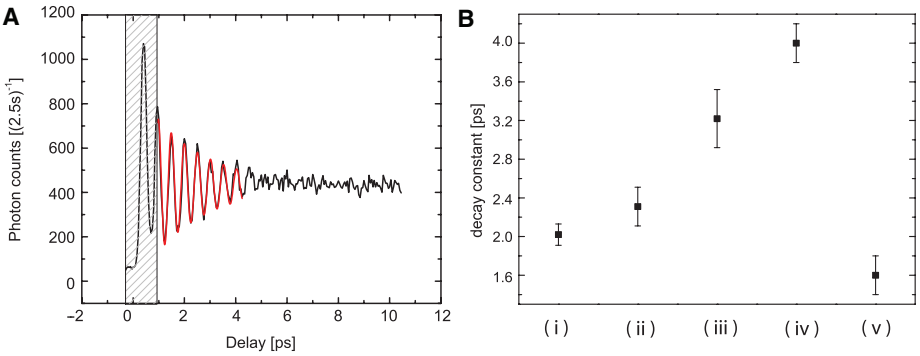

Fig. 3. (**A**) An exponentially damped sine wave (red line) is fitted through the quantum beats outside the control window (cross-hatched box) during which the light field is present. (**B**) The decay time of the quantum beats for several pulse shapes: (i) transform-limited excitation pulses, (ii) pulses found with the genetic algorithm constrained to have flat phase, (iii) pulses found by the genetic algorithm with no constraints, (iv) pulses with -3.1×10^3 fs^2 negative chirp, and (v) pulses with 3.1×10^3 fs^2 positive chirp. The error bars indicate ± SD of the fit.

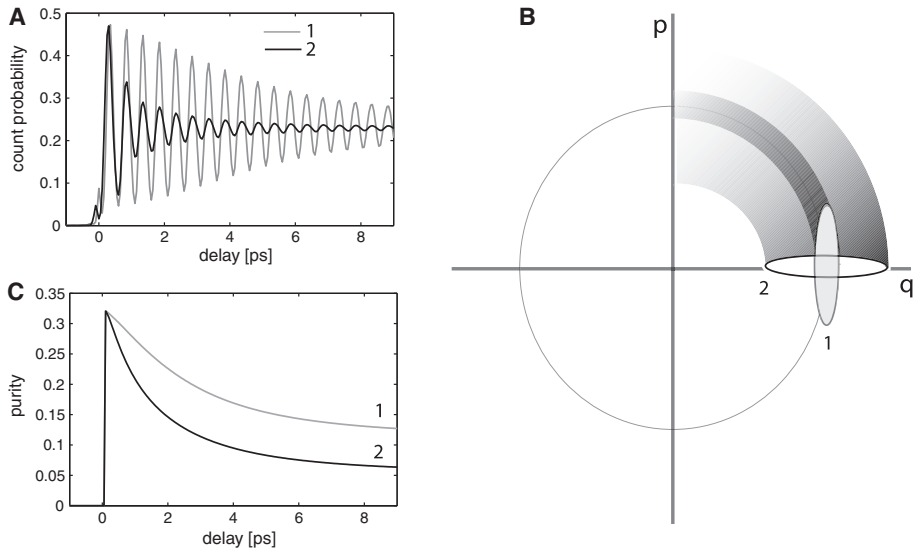

Fig. 4. Illustration of the coherence-preserving mechanism for two states labeled "1" and "2," calculated via the system-bath model. (**A**) The quantum beats decay at different rates for the two states. (**B**) The dephasing spreads the phase-space distribution along the classical trajectory (gray circle). The coherence lifetime is extended if the orientation in phase space of the initial state is along the classical trajectory. (**C**) The total uncertainty in phase space remains smaller for phase-space distribution 1 (representing state 1) than for phase-space distribution 2 (representing state 2), and consequently the purity decays less rapidly.

Downloaded from www.sciencemag.org on May 8, 2008

the Hamiltonian $\hat{H}_i$ of a diatomic molecule in a particular electronic state $|i\rangle$ has the form

$$\hat{H}_i = \frac{\hat{p}^2}{2\mu} + U_i(\hat{q}) + \frac{\hat{\mathbf{J}}^2}{2\mu\hat{q}^2} \quad (1)$$

where $\hat{p}$ and $\hat{q}$ are the internuclear momentum and position operators, μ is the reduced mass, $U_i(\hat{q})$ is the adiabatic vibrational potential of the state $|i\rangle$, and $\hat{\mathbf{J}}$ is the angular momentum operator of the molecule. This system can be analyzed completely in terms of the known eigenstates or in terms of a system-bath model (*30*). Both models reveal that in the position-momentum phase space of the vibrational mode, the effect of the rotational dephasing is to smear the vibrational wave packet along the closed classical trajectory of the oscillations. The area of phase space occupied by a quantum state is simply related to its purity. Therefore, vibrational states whose phase-space distributions are predominantly oriented along the classical trajectory will experience a less rapid growth in the uncertainty product $\Delta q \Delta p$, and thus a less rapid decay of purity, than states of similar initial phase space area whose distributions are oriented orthogonal to the classical trajectory (Fig. 4). Experimentally, we find that pulses with negative chirp produce wave packets that are radially squeezed in phase space (*34*) and thus preserve the purity. Thus, control of the relative phases of the basis states in a coherent quantum superposition provides a natural means to counteract the dephasing process. This simple picture also suggests the limit of possible improvement: If the chirped excitation pulse is as long as one vibrational period (about 500 fs), the initial phase-space distribution is smeared out over 2π, and the purity cannot decay further. However, this completely delocalized state does not show fluorescence quantum beats and so is not controllable via our strategy. The full-model calculation also shows that if the chirp becomes larger, the initial purity is lower than that for the transform-limited pulse, so the optimal solution is a trade-off between a state with very long–lived coherence and one that shows clear localization. Our CS effectively mediates between these limits.

The physical mechanism by which these tailored pulse shapes mitigate dephasing entails control of the fluctuations in the molecules' moment of inertia, which determine the strength of coupling between the rotational and the vibrational degrees of freedom. Negatively chirped pulses generate wave packets that directly reduce the effect of the centrifugal coupling term in Eq. 1. A system-bath model derived from Eq. 1 confirms that the control loop correctly identifies the wave packet shapes that are most resistant to dephasing (*29*). The model shows that position-squeezed vibrational states are approximate eigenstates of the interaction Hamiltonian. The smaller the position variance immediately after excitation, the less the state is affected by the bath coupling. Although the transform-limited pulse produces the vibrational wave packet with equal position and momentum uncertainties, negatively chirped optical control pulses generate squeezed-state wave packets whose position variance is decreased at the cost of increased momentum variance.

The second most important component of the closed-loop search outcome was a sequence of subpulses. When consecutive subpulses are separated by one vibrational period, such a sequence creates constructive interference of multiple wave packets at the target time. These interferences increase the dephasing rate only by a small amount and are an epiphenomenon of our choice of CS.

The time-evolution of the purity of vibrational quantum states excited by optical control pulses may be calculated numerically via Eq. 1 by making use of the known rotational-vibrational spectra and the measured electric field of the excitation pulse. This calculation confirms that the fluorescence quantum-beat visibility is a reasonable surrogate for purity, and thus for quantum coherence, because the purity lasts longer for negatively chirped excitation pulses than for the transform-limited pulse. The calculation of the complete ro-vibrational density matrix is numerically expensive and takes typically several hours because of the dimensionality of the combined system-reservoir Hilbert space. Further, maximizing the purity P of the system state is not a convex problem, so it is not possible to guarantee that solutions are globally optimal. As a separate calculation, we replaced the anharmonic vibrational potentials with harmonic ones. The computed quantum-beat visibility and purity show the same qualitative behavior in both cases, and we conclude that the anharmonicity of the adiabatic Born-Oppenheimer potentials does not play an essential role in this experiment. Our measurements do not distinguish between Hamiltonian delocalization and decoherence, and therefore our control strategy would be problematic if anharmonic collapse and rotational dephasing took place on the same time scale; a different CS should be chosen in that case. In other cases where the anharmonicity is large and the anharmonic collapse is rapid as compared with the dephasing, one could optimize the quantum-beat visibility at the first anharmonic full revival. Given the effectiveness of the CS used here, we speculate that any experimentally accessible measure of coherence would form a potential surrogate for use as a control signal. For example, standard time-domain nonlinear optical measurements depend on off-diagonal density matrix elements of the quantum state and thus could also be used as a CS.

We have shown experimentally that control of dephasing by closed-loop methods is a viable approach to reducing the susceptibility of coherent superpositions of quantum states to the effect of an environment. We chose a system sufficiently complex to exhibit generic dephasing dynamics and yet appropriately simple to lend itself to theoretical analysis. Therefore, we were able to numerically simulate the experiment and understand a posteriori the decoherence-preserving mechanism. In more complex systems, this degree of analysis will not be possible. Also, it will be impossible to conceive of an a priori design strategy, especially if the environmental couplings are not known. In contrast, closed-loop control is almost universally applicable and often the only practical way of controlling the coherence of the quantum system. The key to achieving the coherence preservation is to identify a CS that is simple to measure in the laboratory. A direct determination of the purity of the quantum state requires too much data to make it an effective feedback signal for the control loop. With an easily measurable surrogate, the closed-loop method enables the protection of coherence in a system by successfully identifying states that are most immune to dephasing. We expect that this strategy will also be effective at finding true decoherence-free states, where such states exist. In situations where one or more decoherence-free states are available, the search algorithm will be able to locate them, again without the use of previous knowledge of the system-environment couplings. The outcome of our experiment is that appropriately constructed wave packets containing more coherence—in the sense of a larger number of off-diagonal elements of the density matrix in the bare system basis—preserve their coherence longer in the presence of environmental noise than wave packets with fewer populated basis states. Of course, a correct phasing of the states in the quantum superposition is crucial for rendering the wave packet less susceptible to dephasing. Thus, it appears that coherence may be used to fight decoherence: a rather unexpected result, but one that may have implications for other quantum systems and for applications demanding control of quantum interferences.

References and Notes

1. R. S. Judson, H. Rabitz, *Phys. Rev. Lett.* **68**, 1500 (1992).
2. T. C. Weinacht, J. Ahn, P. H. Bucksbaum, *Nature* **397**, 233 (1999).
3. J. L. Herek, W. Wohlleben, R. J. Cogdell, D. Zeidler, M. Motzkus, *Nature* **417**, 533 (2002).
4. T. Brixner *et al.*, *Phys. Rev. Lett.* **92**, 208301 (2004).
5. A. Lindinger *et al.*, *Phys. Rev. Lett.* **93**, 033001 (2004).
6. V. I. Prokhorenko *et al.*, *Science* **313**, 1257 (2006).
7. R. Bartels *et al.*, *Nature* **406**, 164 (2000).
8. R. J. Levis, G. M. Menkir, H. Rabitz, *Science* **292**, 709 (2001).
9. T. Laarmann *et al.*, *Phys. Rev. Lett.* **98**, 058302 (2007).
10. H. Lee, Y. Cheng, G. R. Fleming, *Science* **316**, 1462 (2007).
11. A. Ekert, R. Jozsa, *Rev. Mod. Phys.* **68**, 733 (1996).
12. A. Ekert, R. Jozsa, *Philos. Trans. R. Soc. London Ser. A* **356**, 1769 (1998).
13. A. M. Steane, *Phys. Rev. Lett.* **77**, 793 (1996).
14. J. Preskill, *Proc. R. Soc. London Ser. A* **454**, 385 (1998).
15. D. Vitali, P. Tombesi, *Phys. Rev. A* **59**, 4178 (1999).
16. E. A. Shapiro, I. A. Walmsley, M. Yu. Ivanov, *Phys. Rev. Lett.* **98**, 050501 (2007).
17. D. A. Lidar, I. L. Chuang, K. B. Whaley, *Phys. Rev. Lett.* **81**, 2594 (1998).
18. D. J. Tannor, A. Bartana, *J. Phys. Chem. A* **103**, 10359 (1999).
19. S. E. Sklarz, D. J. Tannor, N. Khaneja, *Phys. Rev. A* **69**, 053408 (2004).
20. U. Hohenester, G. Stadler, *Phys. Rev. Lett.* **92**, 196801 (2004).
21. U. Hohenester, *Phys. Rev. B* **74**, 161307(R) (2006).
22. H. Jirari, W. Pötz, *Phys. Rev. A* **74**, 022306 (2006).
23. G. Katz, M. A. Ratner, R. Kosloff, *Phys. Rev. Lett.* **98**, 203006 (2007).

Downloaded from www.sciencemag.org on May 8, 2008

24. M. Grace *et al.*, *J. Phys. B* **40**, S103 (2007).
25. T. Hansson, *Phys. Rev. A* **61**, 033404 (2000).
26. F. A. Bovino *et al.*, *Phys. Rev. Lett.* **95**, 240407 (2005).
27. T. J. Dunn, I. A. Walmsley, S. Mukamel, *Phys. Rev. Lett.* **74**, 884 (1995).
28. T. J. Dunn, J. N. Sweetser, I. A. Walmsley, C. Radzewicz, *Phys. Rev. Lett.* **70**, 3388 (1993).
29. C. Brif, H. Rabitz, S. Wallentowitz, I. A. Walmsley, *Phys. Rev. A* **63**, 063404 (2001).
30. S. Wallentowitz, I. A. Walmsley, L. J. Waxer, Th. Richter, *J. Phys. B* **35**, 1967 (2002).
31. A. J. Ross, P. Crozet, C. Effantin, J. D'Incan, R. F. Barrow, *J. Phys. B* **20**, 6225 (1987).
32. I. A. Walmsley, L. Waxer, *J. Phys. B.* **31**, 1825 (1998).
33. C. Iaconis, I. A. Walmsley, *Opt. Lett.* **23**, 792 (1998).
34. J. Janszky, A. V. Vinogradov, I. A. Walmsley, J. Mostowski, *Phys. Rev. A* **50**, 732 (1994).

35. This work was supported by the Defense Advanced Research Projects Agency (DARPA) QuIST. I.A.W. acknowledges support by the UK Quantum Information Processing Interdisciplinary Research Collaboration (funded by the Engineering and Physical Sciences Research Council) and the European Community under the Integrated Project QAP (funded by the Information Societies Technology directorate as contract no. 015848).

Supporting Online Material

www.sciencemag.org/cgi/content/full/320/5876/638/DC1
Materials and Methods
References

26 December 2007; accepted 12 March 2008
10.1126/science.1154576

Strong Interactions in Multimode Random Lasers

Hakan E. Türeci,[1]* Li Ge,[2] Stefan Rotter,[2]† A. Douglas Stone[2]

Unlike conventional lasers, diffusive random lasers (DRLs) have no resonator to trap light and no high-Q resonances to support lasing. Because of this lack of sharp resonances, the DRL has presented a challenge to conventional laser theory. We present a theory able to treat the DRL rigorously and provide results on the lasing spectra, internal fields, and output intensities of DRLs. Typically DRLs are highly multimode lasers, emitting light at a number of wavelengths. We show that the modal interactions through the gain medium in such lasers are extremely strong and lead to a uniformly spaced frequency spectrum, in agreement with recent experimental observations.

Novel laser systems have emerged recently because of modern nanofabrication capabilities (*1*–*3*). The diffusive random laser (DRL), perhaps the most challenging of the new systems, consists of a random aggregate of particles that scatter light and have gain or are embedded in a background medium with gain (*2*, *4*–*8*). Whereas light scattering in such a random medium can give rise to Anderson-localized, high-Q resonances (*9*, *10*), in almost all experiments the localized regime is not reached, and the laser "cavity" has no isolated resonances in the absence of gain. Despite the lack of sharp resonances, the laser emission from the more recent DRLs (*2*, *5*, *6*) was observed to have the essential properties of conventional lasers: the appearance of coherent emission with line-narrowing above a series of thresholds and uncorrelated photon statistics far from threshold (*11*). Earlier work on random lasers (*4*, *7*) did not find isolated narrow lines and was interpreted as incoherent lasing, in which there was intensity feedback but not amplitude feedback. Later experiments (*2*) and recent numerical studies (*12*) indicated that the lasing involves coherent phase-sensitive feedback in at least some cases. Our work shows that standard coherent multimode lasing is possible even when the linear resonances are much broader than their spacing, raising the question of what determines the emission frequencies of DRLs because they are not determined by the position of passive cavity resonances. Furthermore, recent experiments on porous GaP DRLs have shown that the frequencies are rather uniformly spaced and stable from pulse to pulse, although the intensities vary substantially (*8*). We show that this is a result of strong nonlinear interactions between lasing modes combined with extreme leakiness, a regime particularly difficult to treat. In any multimode laser, the different modes compete with one another through the gain medium in a complex manner that depends on the spatial distribution of the electric field of each mode. This is particularly severe in the DRL, in which there are many spatially overlapping modes with similar (very short) lifetimes.

The finesse, f, of a resonator is defined as the ratio of the resonance spacing to the resonance width; standard laser theory only addresses lasers with high finesse (weakly open) resonators and cannot be applied to the DRL, which has finesse much less than unity. Hence, no analytic results have been derived relating to two-dimensional (2D) or 3D DRLs, and realistic numerical simulations have been limited because of the computational demands. We introduced a formulation of semiclassical laser theory in terms of biorthogonal modes, called constant flux (CF) states, which treats lasing media with any degree of outcoupling and includes the effects of nonlinear modal interactions to all orders (*13*, *14*). We present analytic and numerical results using this approach applied to a DRL.

The simplest model for a laser that captures all of the relevant spatial complexity uses the Maxwell-Bloch equations (*15*, *16*), which are three coupled nonlinear equations for the electric field, the polarization, and the inversion of the gain medium. For stationary multimode lasing, the modes predicted by these equations are determined by the time-independent self-consistent equation (*13*)

$$\Psi_\mu(\boldsymbol{x}) = \frac{i\gamma_\perp}{\gamma_\perp - i(k_\mu - k_a)} \int dx' \frac{D_0(\boldsymbol{x}) G(\boldsymbol{x},\boldsymbol{x}';k_\mu)\Psi_\mu(\boldsymbol{x}')}{\varepsilon(\boldsymbol{x}')\left(1+\sum_\nu \Gamma_\nu |\Psi_\nu(\boldsymbol{x}')|^2\right)} \quad (1)$$

where the electric field is given by $e(\boldsymbol{x},t) = \sum_\mu \Psi_\mu(\boldsymbol{x}) e^{-i\Omega_\mu t}$. In Eq. 1, the lasing frequencies $\Omega_\mu = ck_\mu$ and the lasing mode functions $\Psi_\mu(\boldsymbol{x})$ are assumed to be unknown (henceforth we set the speed of light $c = 1$ and use the wave vector to denote frequency as well). In Eq. 1, k_a is the atomic frequency, $\gamma_\perp$ is the transverse relaxation rate, $\Gamma_\nu = \Gamma(k_\nu)$ is the gain profile evaluated at k_ν, $D_0(\boldsymbol{x}) = D_0\,[1 + d_0(\boldsymbol{x})]$ is the pump, which can vary in space, and $\varepsilon(\boldsymbol{x}) = n^2(\boldsymbol{x})$ is the dielectric function of the "resonator." Electric field and pump strength are dimensionless, being measured in units $e_c = \hbar\sqrt{\gamma_\perp\gamma_\parallel}/2g$ and $D_{0c} = 4\pi k_a^2 g^2/\hbar\gamma_\perp$, where $\gamma_\parallel$ is the longitudinal relaxation rate and g is the dipole matrix element of the gain medium. Each lasing mode Ψ_μ depends nonlinearly on all of the other lasing modes through the denominator in Eq. 1, which represents the "spatial hole-burning" (*15*) interaction with the other modes. Through this mechanism, modes that lase first tend to suppress lasing in other modes, particularly those with which they are correlated in space.

For simplicity we study a 2D DRL and take the gain medium to be a uniform disk of radius R, which contains randomly placed nanoparticles with constant index greater than unity. The light field in the cavity can be either transverse magnetic or transverse electric polarized perpendicular to the plane of the disk, leading to a scalar equation for its normal component. The integral in Eq. 1 is over the gain region, and the kernel $G(\boldsymbol{x},\boldsymbol{x}';k)$ is the Green function of the cavity wave equation with purely outgoing boundary conditions (*13*). This represents the steady-state response of the passive cavity to a monochromatic dipole oscillating with frequency k at $\boldsymbol{x}'$. The nonhermitian boundary conditions on the Green function lead to a spectral representation $G(\boldsymbol{x},\boldsymbol{x}';k)$ in terms of dual sets of biorthogonal functions $\varphi_m(\boldsymbol{x}, k)$ and $\overline{\varphi}_m(\boldsymbol{x}, k)$, termed constant flux (CF) states, with complex eigenvalues, k_m (*13*).

The CF states play the role of the linear cavity resonances within our theory and reduce to the quasi-bound (QB) states within the cavity to a

[1]Institute of Quantum Electronics, Eidgenössische Technische Hochschule (ETH) Zurich, 8093 Zurich, Switzerland. [2]Department of Applied Physics, Post Office Box 208284, Yale University, New Haven, CT 06520–8284, USA.

*To whom correspondence should be addressed. E-mail: tureci@phys.ethz.ch

†Presently on leave from Technische Universitat Wien, Wiedner Hauptstraße 8-10/136, A-1040 Vienna, Austria.

Downloaded from www.sciencemag.org on May 8, 2008